Solution Small-Angle X-ray Scattering Study of the Molecular Chaperone Hsc70 and Its Subfragments†

Sigurd M. Wilbanks,‡,§ Lingling Chen,‖,§ Hirotsugu Tsuruta,⊥ Keith O. Hodgson,‖ and David B. McKay*,‡

Beckman Laboratories for Structural Biology, Department of Structural Biology, Stanford University School of Medicine, Stanford, California 94305-5400, Department of Chemistry, Stanford University, Stanford, California 94305-5080, and Stanford Synchrotron Radiation Laboratory, Stanford, California 94305

Received June 20, 1995⊗

ABSTRACT: Solution X-ray scattering experiments have been carried out on recombinant bovine Hsc70 (with 650 amino acid residues), a 60 kDa subfragment (residues 1−554) which has ATPase- and peptide-binding activities, a 44kDa subfragment (residues 1−386) which has only ATPase activity, and a peptide-binding fragment (residues 388−554). Modeling based on steady-state values of radii of gyration (R_g's) and $P(r)$ functions shows that the 44 kDa and peptide-binding domains are oblate fragments while Hsc70 and the 60 kDa fragment are prolate and relatively elongated. R_g values decrease significantly in the presence of MgATP relative to their values in the presence of MgADP (ΔR_g ~4−5 Å) for Hsc70 and the 60 kDa fragment; in contrast, they are essentially equal in the presence of either nucleotide for the 44 kDa ATPase fragment. The kinetics of the change of R_g for Hsc70 and the 60 kDa fragment under single-ATPase cycle conditions show that the transition to the ATP-induced R_g occurs significantly more rapidly than ATP hydrolysis while the reverse transition to the larger R_g value does not occur before product release. Altogether, the solution scattering data support a model in which a conformational change in Hsc70 (presumably to the low-peptide-affinity state) is predicated on ATP binding while the reverse transition is predicated on product release.

The 70 kDa heat shock-related ("stress-70") proteins comprise a family of highly conserved molecular chaperones that are necessary for cell viability in all organisms. The bovine heat shock cognate protein (Hsc70)[1] is a constitutively expressed member of this family; it was originally isolated and characterized as a protein with an *in vitro* clathrin-uncoating activity (Schlossman *et al.*, 1984; Chappell *et al.*, 1986). It has subsequently been implicated in transmembrane targeting of proteins (Chirico *et al.*, 1988; Deshaies *et al.*, 1988) and has been found associated with nascent polypeptides during translation (Beckmann *et al.*, 1990; Scherer *et al.*, 1990; Langer *et al.*, 1992). The stress-70 proteins are thought to bind unstructured polypeptides and (partially or fully) denatured proteins *in vivo*, thereby suppressing their aggregation (Pelham, 1986; Gething & Sambrook, 1992). *In vitro* studies have shown that stress-70 proteins bind both denatured proteins (but not their native counterparts) and some short (≥7 residues) synthetic peptides and that these (poly)peptides are released in response to addition of MgATP (Flynn *et al.*, 1989, 1991; Blond-Elguindi *et al.*, 1993; Gragerov *et al.*, 1994).

Fluorescence, proteolysis, and circular dichroism studies have shown that DnaK, the *Escherichia coli* representative of the stress-70 family, undergoes a significant conformational change upon addition of MgATP (Liberek *et al.*, 1991; Palleros *et al.*, 1992). It has been shown that binding of MgATP in the presence of K^+ is required for release of denatured proteins from several different purified stress-70 proteins (Schlossman *et al.*, 1984; Palleros *et al.*, 1993). These data suggest that the conformational change that results from the addition of MgATP is the switch that releases bound peptides and denatured proteins *in vitro*. In addition, ATP can dissociate dimers of stress-70 proteins (Schlossman *et al.*, 1984; Freiden *et al.*, 1992; Kim *et al.*, 1992).

Stress-70 proteins have an ATPase activity, a peptide-binding activity, and a mechanism of coupling the two such that addition of MgATP induces peptide release (Palleros *et al.*, 1993). The ATPase activity resides in the amino-terminal ~385 amino acid residues (Chappell *et al.*, 1987). The peptide-binding activity resides within the remainder of the molecule; there is evidence that the carboxy-terminal ~100 amino acids are not required for peptide binding (Chappell *et al.*, 1987; Wang *et al.*, 1993). The three-dimensional structure of the ATPase domain of bovine Hsc70 has been solved (Flaherty *et al.*, 1990); it is strikingly similar to the tertiary structure of actin (Flaherty *et al.*, 1991). Determination of secondary structure of the peptide-binding domain of rat Hsc70 by NMR has also been reported (Morshauser *et al.*, 1995).

To develop a low-resolution model for Hsc70, to determine the magnitude of and the nucleotide requirements for the

† This work was supported by NIH Grant GM-39928 to D.B.M. Operation of beamline 4-2 and the Stanford Synchrotron Radiation Laboratory (SSRL) are supported by the Department of Energy, Office of Basic Energy Sciences, Division of Chemical Sciences. Additional support to SSRL is provided by the NIH National Center of Research Resources Biochemical Research Technology Program (RR-01209), Division of Research Resources, and by the Department of Energy, Office of Health and Environmental Research.

* Author to whom correspondence should be addressed.
‡ Stanford University School of Medicine.
‖ Stanford University.
⊥ Stanford Synchrotron Radiation Laboratory.
§ These two authors contributed equally to this work.

⊗ Abstract published in *Advance ACS Abstracts,* September 1, 1995.

[1] Abbreviations: AMPPNP, 5′-adenylyl-β,γ-imidodiphosphate; Hsc70, constitutively expressed stress-70 protein; MOPS, 3-(*N*-mopholino)-propanesulfonic acid; PMSF, phenylmethanesulfonyl fluoride; R_g, radius of gyration; SAXS, small angle X-ray scattering; stress-70, 70 kDa heat shock-related.

0006-2960/95/0434-12095$09.00/0

ATP-induced conformational change, and to attempt to correlate the conformational change with specific steps of the enzymatic ATPase cycle, we have carried out solution small-angle X-ray scattering studies of recombinant bovine Hsc70 and its subfragments.

MATERIALS AND METHODS

Expression and Purification of Protein. Full-length recombinant bovine Hsc70 (amino acid residues 1−650), which has ATPase and peptide-binding activities, and the truncation consisting of residues 1−386 ("ATPase fragment") were expressed in *E. coli* as described elsewhere (Wilbanks *et al.*, 1994). The plasmid for expressin of the truncation including residues 1−554 ("60 kDa fragment"), which also has ATPase and peptide-binding activities, was subcloned from the pT7-7-derived plasmid used to express Hsc70. This was achieved by replacing an *Eco*RI/*Sal*I fragment including the codons for residues 540−650, termination signals, and part of the polylinker with a synthetic oligonucleotide encoding residues 540−554 and a termination codon. Using the same procedure, the truncation encoding residues 388−554 ("peptide-binding domain") was subcloned from a pT7-7-derived plasmid that encodes the carboxy-terminal fragment of the protein, residues 388−650 (we are indebted to Melanie O'Brien for providing the latter plasmid). Protein expression was induced in *E. coli* strain BL21(DE3) by addition of isopropylthio β-D-galactoside (0.4 mM final concentration) to log phase cultures.

Purification schemes for Hsc70 and the ATPase fragment were modifications of those published previously (O'Brien & McKay 1993; Wilbanks *et al.*, 1994). Cells were lysed by sonication, and the lysate was cleared by centrifugation at ~16000*g* and applied to a DE-52 anion exchange column (Whatman, Clifton, NJ) equilibrated in 25 mM Tris−25 mM KCl−0.1 mM PMSF, pH 7.0. Hsc70 was eluted with 25 mM Tris−150 mM KCl−0.1 mM PMSF, pH 7.0; the ATPase fragment was eluted with a gradient of 25−200 mM KCl in the same buffer. Both proteins were next purified using an ATP-agarose column (Sigma, St. Louis, MO) as published previously, except that Hsc70 was applied to the ATP-agarose column by batch absorption with rocking for 16 h at 4 °C rather than by conventional loading of a prepoured column. Chromatofocusing over a Mono-P column followed by gel filtration on a Superdex-75 column were used as the final steps of purification (both columns from Pharmacia, Uppsala, Sweden). Final buffer conditions, established on the gel filtration column, were 10 mM MOPS−150 mM KCl, pH 7.0, for the ATPase fragment and 10 mM MOPS−100 mM K(OAc), pH 6.5, for Hsc70.

A variation of this protocol was used to purify the 60 kDa fragment. Since it was not retained on the DE-52 column, it was collected in the flowthrough, applied to a hydroxylapatite column (Bio-Rad, Richmond, CA) equilibrated in 20 mM potassium phosphate−50 mM calcium phosphate−0.1 mM PMSF, pH 7, and then eluted with a gradient of 20−200 mM potassium phosphate, also with calcium and PMSF at pH 7. Chromatofocusing and gel filtration were carried out as described above; the 60 kDa protein was stored in 10 mM MOPS−150 mM KCl, pH 7.0.

Cells expressing the peptide binding domain were harvested and lysed in the same fashion, and the lysate was cleared by centrifugation. The supernatant fraction from that spin was brought to 40% saturation with $(NH_4)_2SO_4$, the resulting precipitate was removed by centrifugation, the supernatant fraction was brought to 60% saturation with $(NH_4)_2SO_4$, and the resulting precipitate was again removed by centrifugation. The supernatant fraction, containing the majority of the peptide-binding domain, was applied to a phenyl-sepharose column (Sigma, St. Louis, MO) equilibrated in 2 M $(NH_4)_2SO_4$−20 mM Bis−Tris propane, pH 7, eluted with 0.6 M $(NH_4)_2SO_4$ −20 mM Bis-Tris propane, pH 7, and precipitated by addition of $(NH_4)_2SO_4$ to near saturation. Resuspended protein was filtered and chromatographed by gel filtration on a Superdex-75 column in 10 mM MOPS−100 mM K(OAc), pH 7.

Kinetic Assays. Kinetic rate constants for ATP hydrolysis, product release, and steady-state ATPase turnover were determined for the 60 kDa fragment at 25 °C, in the presence of 10 mM MOPS−4.5 mM $Mg(OAc)_2$−150 mM KCl, pH 7, using methods described previously (Ha & McKay, 1994).

The rate constant for ATP hydrolysis was determined under single-turnover conditions (1 or 2 μM 60 kDa fragment, 10 nM [α-^{32}P]ATP). Aliquots of the reaction mixture were withdrawn at specific time points, quenched with acid, and neutralized, and the α-^{32}P-labeled adenosine nucleotides were separated by thin layer chromatography. The relative amount of each radioactive nucleotide was determined with a PhosphorImager system (Molecular Dynamics, Sunnyvale, CA), and the fraction hydrolyzed was computed as the ratio of counts in the ADP spot to the sum of counts in both ADP and ATP spots (after correction for background). Data on the fraction of ATP hydrolyzed versus time were fit with a single exponential, yielding the hydrolysis rate constant.

The rates of release of products were determined using filter binding assays described previously (Ha & McKay, 1994). To determine the rate of ADP release, protein was first incubated with stoichiometric amounts of [α-^{32}P]ATP for sufficient time to allow complete hydrolysis (>6 × hydrolysis half-life). Then, an excess of unlabeled ATP was added, and the amount of label released from the protein was followed as a function of time; concentrations after addition of unlabeled ATP were 2 mM protein and 100 mM ATP. Aliquots were withdrawn from the reaction and filtered immediately through BA-85 nitrocellulose membranes (Schleicher & Schuell, Keene, NH); filters were then washed briefly with buffer, dried, and counted by Cherenkov counting. A rate was inferred from a single-exponential fit to the data. To determine the rate of release of P_i, reactions were initiated by mixing [γ-^{32}P]ATP to 10 nM with 10 mM protein, and the release of $^{32}P_i$ was monitored by filter binding. The rate constant for P_i release was extracted from the data using methods described previously which taken into account the effect of ATP hydrolysis on the apparent release rate (Ha & McKay, 1994).

Steady-state hydrolysis rates were determined in reactions containing 40 or 400 nM enzyme and 4 μM [α-^{32}P]ATP in the same buffer as for single-turnover reactions. Separation and measurement of ATP and ADP were by TLC and PhosphorImager instrument as described above. The hydrolysis rate was computed as the slope of a linear fit to data representing the fraction of ATP hydrolyzed versus time.

Preparation of Protein Samples for Solution Scattering. Hsc70 and the peptide-binding domain aggregate significantly when left in solution at high (~10 mg/mL) concentra-

tions for an extended (days) period of time. To circumvent this problem, samples of these proteins used for scattering measurements were rendered aggregate-free by gel filtration within 24 h of their use, and measurements were made at concentrations less than 4 mg/mL (for Hsc70) or 8 mg/mL (peptide-binding fragment). This precaution was not necessary for the ATPase and 60 kDa fragments, since they had less propensity to aggregate. Protein concentrations were determined spectrophotometrically, using calculated molar extinction coefficients at $\lambda = 280$ nm of 30 800, 23 700, 18 600, and 5100 M^{-1} cm^{-1} for Hsc70, 60 kDa fragment, ATPase fragment, and peptide-binding domain, respectively. The molecular weights of these species were calculated to be 71.2, 61.0, 42.5, and 18.4 kDa, respectively. Samples were judged to be nucleotide-free based on an A_{280}/A_{260} ratio of >1.4. Where necessary, nucleotide was removed from protein by charcoal extraction as described previously (Ha & McKay, 1994).

Nondenaturing polyacrylamide gels were 7%, with 4% glycerol present (Kim *et al.*, 1992). Dynamic light scattering was measured on a Biotage dp801 molecular size detector using samples filtered through 0.02 μm filters.

Chicken egg white lysozyme (Sigma, St. Louis, MO) used in scattering experiments was dialyzed against 40 mM NaOAc−150 mM NaCl, pH 3.8, and the protein concentration was determined spectrophotometrically using $\epsilon_{280} = 2.64$ mg^{-1} cm^{-1} mL.

Data Collection. X-ray solution scattering experiments were performed on beamline 4-2 of the Stanford Synchrotron Radiation Laboratory in March 1994, June 1994, and March 1995 using the resident SAXS camera (Wakatsuki *et al.*, 1992). The X-ray source (SPEAR) was operated at 3.0 GeV and 60−100 mA. Radiation of wavelength at 1.38 Å was selected with a double-crystal Si[111] monochromator and collimated with a rectangular two-slit system to dimensions 1.0 mm (in the plane of diffraction) by 2.1 mm (perpendicular to the plane of diffraction) at the sample. A Pt-coated mirror was used to reject higher order harmonics in the March 1994 and June 1994 runs and additionally as a focusing mirror in the March 1995 run. Incident beam intensity was monitored using an ionization chamber positioned immediately before the sample chamber. Both a linear detector (a one-dimensional position-sensitive proportional counter; Bio-Logic, Grenoble, France) and a quadrant detector (developed at EMBL, Grenoble) were used in separate experiments. The linear detector was filled with 80% xenon/20% carbon dioxide and was operated at 1.8−1.9 kV during the experiments; the quadrant detector was filled with 70% argon/30% carbon dioxide and was operated at 3.4 kV. Sample-to-detector distance was determined from the diffraction pattern of a cholesterol myristate powder sample and was found to be 234 ± 1 cm for the linear detector and 238 ± 1 for the quadrant detector. The linear detector covered the scattering range $0.002 < S < 0.03$ Å^{-1} ($S = 2 \sin \theta/\lambda$, where 2θ = scattering angle and λ = X-ray wavelength), and the quadrant detector covered $0.005 < S < 0.04$ Å^{-1}. Detector response was calibrated every 6−12 h using a homogenous field of radiation, from either a copper fluorescence (for the linear detector) or an ^{55}Fe source (for the quadrant detector).

Sample cells were Kel-F or Macor (Corning, Corning, NY) blocks with a 25−30 μL sample chamber, 1.2 mm path length, and 10 μM thick mica windows. The temperature of the cell was controlled by circulating ethylene glycol from a temperature-controlled bath through the jacket of the cell holder.

During the March 1994 and June 1994 runs, data collection from each sample was limited to 10 min, divided into either 5 cycles of 2 min or 10 cycles of 1 min, since cumulative exposure times significantly greater than 10 min resulted in an upswing of the scattering curve at low angle, indicative of radiation-induced sample deterioration. During the March 1995 run, it was found that deterioration could be retarded by addition of 20 mM β-mercaptoethanol to the protein samples, allowing data collection time to be extended to 20 min. Background scattering was recorded either immediately before or immediately after each protein sample using the same sample cell filled with the corresponding buffer and nucleotide solution. Multiple samples were used under each set of conditions, and their results were averaged, in order to improve statistical precision in the final results. Typical scattering curves for the 60 kDa fragment are shown in Figure 1. Representative samples that were recovered and assayed for ATPase activity after data collection were found to be enzymatically active.

Data Reduction and Analysis. The SSRL program suite ANOM was used for data reduction (Rice & Wakatsuki, 1991). Each data cycle was normalized to the incident beam intensity and examined for obvious anomaly, such as failure of the system to record the data or radiation-induced aggregation; anomalous sets of data amounted to fewer than 0.5% of all data and were discarded. Repetitive cycles of data collected on each sample were averaged, and the measured background scattering profile was subtracted. A detector response correction was applied as a channel-by-channel division of the data by the detector response (integrated intensity for each channel) to a uniform field of radiation. For data collected with the linear detector, the two scattering curves from opposite sides of the direct beam were averaged.

Radii of gyration (R_g's) were extracted from linear detector data with two different methods. First, a value of R_g for each sample was computed using the Guinier approximation (Guinier, 1963):

$$\ln(I/I_0) = -\frac{(2\pi S R_g)^2}{3}$$

where I is the scattered intensity and I_0 is the intensity at zero angle. This equation was fit to data over a range of $0.0032 < S < 0.0065$ Å^{-1} for samples of Hsc70 or 60 kDa fragment and over $0.0032 < S < 0.0095$ Å^{-1} for samples of ATPase fragment or peptide-binding domain.

Second, a pair distribution function,

$$P(r) = 8\pi r \int_0^\infty dS \cdot S \cdot I(S) \cdot \sin(2\pi S r)$$

(where $I(S)$ = scattered intensity at S), was calculated using the indirect transformation method of Svergun, as implemented with the GNOM program package (Semenyuk & Svergun, 1991), with data over the angular range $0.0026 < S < 0.0280$ Å^{-1}. R_g and d_{max}, the minimum distance at which $P(r) = 0$, were then calculated from the $P(r)$ function.

Data collected to higher angle on the quadrant detector were combined with data from equivalent samples collected on the linear detector by linearly scaling the two separate

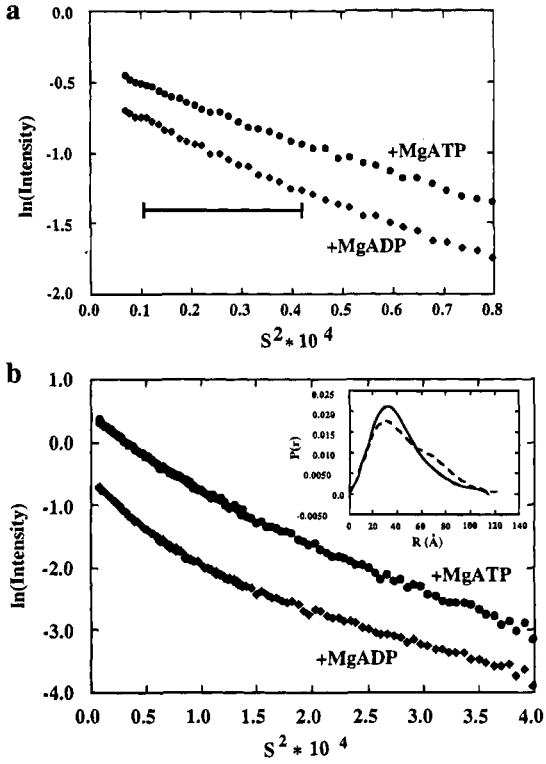

FIGURE 1: Scattering curves from linear detector, plotted as ln(I) versus S^2, for the 60 kDa fragment in the presence of MgADP (◆) and MgATP (●), (a) at low angle and (b) an extended region. Horizontal bar in panel a shows region used to compute R_g in the Guinier approximation. Insert in panel b shows the $P(r)$ functions (solid line, MgATP; dashed line MgADP) computed from data from both detectors. For clarity, the scattering curve collected with MgATP is shifted vertically from that collected with MgADP in both figures.

datasets to achieve the best fit in the range $0.008 < S < 0.012$ Å^{-1}. The $P(r)$ function was then computed from the combined scattering curve, using data over the angular range $0.0026 < S < 0.0280$ Å^{-1}. This function was used in the modeling studies.

RESULTS

Reproducibility of Data and Accuracy of R_g Values. Both Guinier analysis and $P(r)$ function analyses were used to extract estimates of R_g from experimental scattering curves. Representative scattering curves are shown in Figure 1. For the smaller protein constructs (ATPase and peptide-binding fragments), the maximum values of $2\pi S \cdot R_g$ used in the Guinier analysis ranged 1.1−1.3, and the R_g values computed (i) using the Guinier approximation and (ii) using the $P(r)$ function agree within experimental error (Table 1). For the larger proteins (Hsc70 and the 60 kDa fragment), R_g's computed from $P(r)$ functions were systematically ~2 Å larger than those computed using the Guinier analysis, and maximum values of $2\pi S \cdot R_g$ used in the Guinier analysis ranged 1.1−1.5. The disagreement between R_g's calculated by the two methods may be due to the use of a relatively generous Guinier region for the larger proteins, which was necessitated by the fact that restricting the analysis to smaller scattering angles (*e.g.*, $2\pi S \cdot R_g < 1.0$) reduced the number of data points included in the linear fit to fewer than 12 in some cases, at which point the errors in the detector response correction of individual channels significantly affected the calculated slope of the linear fit used for Guinier analysis.

In order to assess the combined reproducibility of the sample preparation protocols and the experimental apparatus, complete datasets were taken on two separate runs for each of the protein constructs (Table 1). Pairs of R_g values determined on the same construct on different runs generally agreed within computed error (*i.e.*, the standard deviation of the intercept value of a weighted linear fit to experimental values of R_g versus concentration); for example, the two values of R_g for the ATPase domain in the presence of MgADP differed by 0.3 ± 0.3 Å. The greatest variation was observed with Hsc70 in the presence of ADP, where differences between values from two independent determinations of R_g were 2.6 ± 1.2 Å in the Guinier approximation or 3.2 ± 0.7 Å by $P(r)$ function analysis. This correlates with conditions where Hsc70 shows the greatest propensity to aggregate in solution and presumably reflects heterogeneity at the biochemical level, since variations of this magnitude did not occur with other samples. Because of this, an emphasis has been placed in the following discussion on using results from the constructs which are least variable in their behavior (ATPase and 60 kDa fragments) for quantitative modeling and then extending these results to Hsc70 as far as is supported by the data.

Allowing for the variability of results on Hsc70 in the presence of ADP, values of the change of R_g (ΔR_g) between different nucleotide conditions (e.g., with MgATP versus with MgADP) computed by the two different analyses (Guinier and $P(r)$ analyses) agree within statistical error. Consequently, it appears that the ΔR_g values determined from Guinier analyses of low-angle data are as reliable as those computed by incorporating higher angle data into the $P(r)$ function. In the following discussions, Guinier values of R_g are used to parameterize the magnitudes and kinetics of nucleotide-induced conformational changes, as revealed by changes in R_g. To test the validity of using the $P(r)$ function analysis of scattering data to higher angle, comparisons are made below between experimental $P(r)$ functions for the ATPase fragment and those computed from crystallographic coordinates; the agreement between the measured and computed distributions support the assertion that values of R_g derived from the $P(r)$ function will be accurate.

Steady-State Radii of Gyration. The linear detector was used to record scattering curves from samples of Hsc70 in the concentration range 1−4 mg/mL (14−57 μM) in the presence of 0.5 mM MgATP or MgADP. For MgATP, this concentration is well above the K_m of steady-state hydrolysis (~0.1 μM), and the nucleotide:protein ratio is such that less than 5% of the ATP will be hydrolyzed during the course of the measurements. For MgADP, this concentration is well above the K_d of the nucleotide (0.11 μM). In the presence of either MgATP or MgADP, the apparent R_g increases slightly with increasing protein concentration (Figure 2a), suggesting that a small amount of aggregation may be present at the higher protein concentrations.

The R_g measured in the presence of MgATP is substantially smaller than that measured in the presence of MgADP at all concentrations (Figure 2a and Table 1). Extrapolation of R_g to zero protein concentration gives values of ~36 Å in the presence of MgADP and ~33 Å in the presence of saturating amounts of MgATP, suggesting that MgATP induces a significant conformational change in Hsc70, relative to its conformation in the presence of MgADP. The concentration-normalized values of $I(0)$ are the same in the

Table 1: Steady-State Structure Parameters (Å) Derived from Solution Scattering Data for Hsc70, the 60 kDa Fragment, and the 44 kDa ATPase Domain in the Presence of MgADP and MgATP and the Peptide-Binding Fragment[a]

	in the presence of 0.5 mM MgADP			in the presence of 0.5 mM MgATP				
	R_g			R_g			R_g(ADP) − R_g(ATP)	
protein	Guinier	$P(r)$	d_{max}	Guinier	$P(r)$	d_{max}	Guinier	$P(r)$
Hsc70	34.9 ± 0.2[b]	38.5 ± 0.5[b]		32.8 ± 0.3[b]	34.7 ± 0.8[b]		2.1 ± 0.3[b]	3.8 ± 0.9[b]
	37.5 ± 1.0[c]	41.7 ± 0.5[c]	130[d]	33.4 ± 0.2[c]	34.5 ± 0.6[c]	120[d]	4.1 ± 1.0[c]	7.2 ± 0.8[c]
60 kDa fragment	32.3 ± 0.1[b]	34.0 ± 0.1[b]		26.9 ± 0.3[b]	28.7 ± 0.5[b]		5.4 ± 0.3[b]	5.3 ± 0.5[b]
	31.3 ± 0.5[c]	34.5 ± 0.4[c]	125[d]	26.4 ± 0.9[c]	29.6 ± 1.0[c]	115[d]	4.9 ± 1.0[c]	4.9 ± 1.1[c]
ATPase domain	22.8 ± 0.2[b]	22.6 ± 0.2[b]		22.6 ± 0.1[b]	22.2 ± 0.2[b]		0.2 ± 0.3[b]	0.4 ± 0.2[b]
	23.1 ± 0.2[e]	22.9 ± 0.2[e]	70[d]			70[d]		

	R_g		
	Guinier	$P(r)$	d_{max}
peptide-binding domain	18.3 ± 0.7[b]	18.3 ± 1.0[b]	60−65[d]
	19.1 ± 0.3[e]	19.8 ± 0.1[e]	

[a] Values for R_g are extrapolations to zero protein concentration from values determined at several concentrations, either by Guinier analysis or from $P(r)$ functions. [b] Data derived from March 1994 run. [c] Data derived from June 1994 run. [d] Derived from combined data of linear and quadrant detector, June 1994 run. [e] Data derived from March 1995 run.

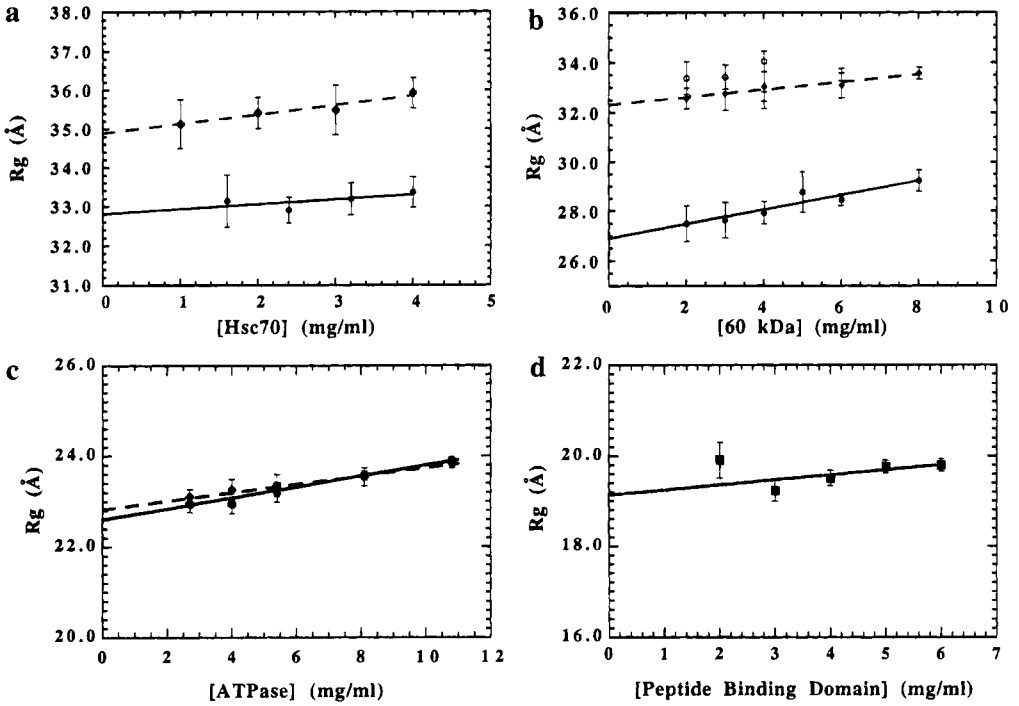

FIGURE 2: Concentration dependence of steady-state R_g computed by Guinier approximation for (a) Hsc70, (b) the 60 kDa fragment, (c) the ATPase fragment, and (d) the peptide-binding domain. For a−c (◆) in the presence of MgADP, (●) in the presence of MgATP, and (○) in the presence of MgATP with Na^+ rather than with K^+. Multiple measurements were taken at every concentration. Errors associated with individual measurement were derived from the least squares fitting of the data in the Guinier regions. The error bar shown at each concentration in the figures is chosen to be the larger value between the maximum of individual errors and the standard deviation from the mean value of different measurements. Solid and dashed lines represent the extrapolation to zero protein concentration in the presence of MgATP and MgADP, respectively. Data for a−c, from March 1994; data for d, from March 1995.

presence of either nucleotide and are consistent with a molecular weight of ~70 kDa, when compared to the $I(0)$ values determined for a standard of known molecular weight, lysozyme. Thus, under both conditions Hsc70 is largely monomeric; the difference in R_g between that observed with MgATP and that observed with MgADP is not due to oligomerization.

Scattering curves were also recorded for Hsc70 at 4 mg/mL in absence of nucleotide (Table 2). The computed R_g shows no statistically significant difference from that with MgADP present. Data were also collected in the presence of 1 mM MgAMPPNP, a slowly hydrolyzable analog of ATP. Again, the computed R_g was equal within experimental error to that observed with MgADP present. Only MgATP was able to induce the conformational change to the smaller R_g in Hsc70.

To test whether the change in R_g could be localized to the nucleotide-binding domain of Hsc70, data were collected and analyzed in the same way from samples containing 1−11 mg/mL ATPase domain (Figure 2c). Extrapolation of R_g to zero concentration yields values of 22.8 Å in the presence of MgADP and 22.6 Å in the presence of MgATP, revealing no detectable difference in conformation between the two states in solution. This is consistent with crystallographic results on wild-type and several mutant proteins which show the ATPase domain to have the same overall conformation

Table 2: Representative R_g Values (Å; Computed in Guinier approximation) for Hsc70, the 60 kDa Fragment, and the 44 kDa ATPase Fragment under Different Nucleotide Conditions[a]

	nucleotides				MgATP	
	MgADP	MgAMPPNP	MgAMPPCP	no nucleotide	Na^+ buffer	K^+ buffer
Hsc70	35.5 ± 0.6[b]	36.8 ± 0.3[b]	ND	37.4 ± 0.4[b]	ND	33.4 ± 0.4[b]
60 kDa fragment	33.1 ± 0.6[b]	32.5 ± 0.3[b]	32.7 ± 0.3[c]	32.6 ± 0.5[c]	34.1 ± 0.4[c]	27.9 ± 0.5[b]
ATPase domain	22.7 ± 0.2[b]	ND	ND		ND	22.5 ± 0.2[b]
	23.1 ± 0.1[d]			23.8 ± 0.1[d]		

[a] Values for Hsc70 and the 60 kDa fragment were determined at a single protein concentration, usually 4 mg/mL, except for the 60 kDa fragment with MgAMPPNP and without nucleotides, where the concentration was 3 mg/mL. Values for R_g of the ATPase fragment are extrapolations to zero concentration. [b] Data derived from March 1994 run. [c] Data derived from June 1994 run. [d] Data derived from March 1995 run. Values not determined are labeled ND.

in the presence of MgATP or MgADP. In the absence of nucleotide, the ATPase domain has a significantly larger R_g at all concentrations, with an increase of 0.6 ± 0.2 Å in the Guinier analysis.

To test whether the 60 kDa fragment, which has both the ATPase domain and the peptide-binding domain, undergoes a conformational change similar to that observed in Hsc70, data were collected and analyzed in a similar manner from samples containing 2−8 mg/mL protein (Figure 2b). The MgATP-containing sample yields a substantially smaller R_g than the sample with MgADP (Table 1). Further, scattering curves were measured and R_g's were computed for several concentrations of the 60 kDa fragment in the absence of nucleotide, in the presence of the slowly hydrolyzable ATP analogs AMPPNP and AMPPCP, and in the presence of MgATP but with Na^+ replacing K^+ in the sample buffer; representative values of R_g determined at 4.0 mg/mL protein concentration are summarized in Table 2. In all cases, the apparent R_g was equal within error to that observed with MgADP present. Thus, the transition to the smaller R_g requires MgATP (slowly hydrolyzable analogs will not substitute) and K^+ (Na^+ will not substitute). Since the 60 kDa fragment shows an ATP-induced conformational change similar to that of Hsc70 and has less tendency to aggregate, many of the subsequent experiments were conducted on it in parallel with experiments on Hsc70.

Scattering curves were also collected for the peptide-binding domain (Figure 2d). Data from two different runs (June 1994 and March 1995) yielded R_g values ~19 Å.

Kinetics of the ATPase Cycle of the 60 kDa Fragment. The rate of ATP hydrolysis was measured for the 60 kDa fragment under single-turnover conditions, using experimental protocols and data analysis methods described previously (Ha & McKay, 1994). Fit of a single exponential to data for the fraction of ATP hydrolyzed versus time yielded a rate of 0.0017 ± 0.0001 s^{-1} ($t_{1/2}$ = 7 min, Figure 3b). When protein is mixed with stoichiometric amounts of [γ-^{32}P]ATP and the release of inorganic phosphate after binding and hydrolysis of the nucleotide was followed, it did not differ significantly from the rate of hydrolysis, demonstrating that phosphate release occurs rapidly after, and is significantly faster than, hydrolysis. The rate of dissociation of ADP from complexes of the 60 kDa fragment preincubated with [α-^{32}P]-ATP for a sufficiently long time to allow complete hydrolysis was measured to be >0.008 s^{-1}. The steady-state ATPase rate was measured to be 0.0024 ± 0.0002 s^{-1}. These data show that under the conditions of our experiments (T = 25 °C), ATP hydrolysis is the rate-limiting step of the ATPase cycle for the 60 kDa fragment. The low hydrolytic rate (in light of the steady-state turnover rate) probably reflects

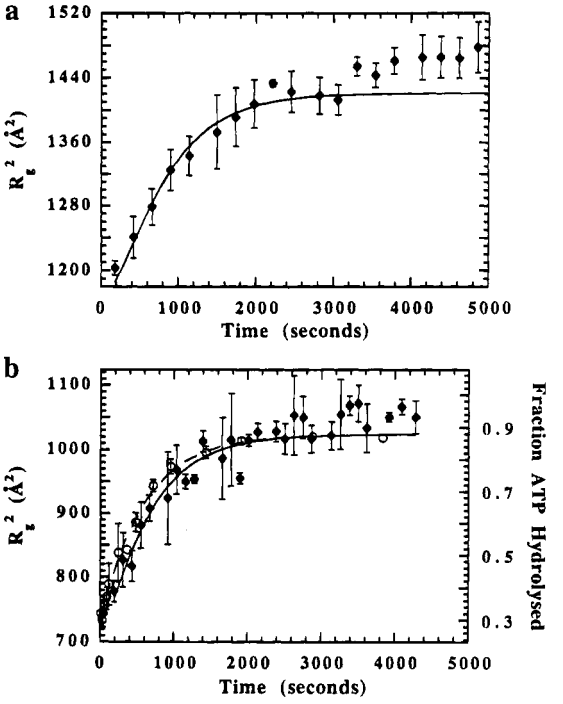

FIGURE 3: Time dependence of R_g^2 after mixing 80 μM protein and 65−75 μM ATP at 25 °C. R_g^2, computed in Guinier approximation, is shown as solid diamonds; each time point represents the average of three separate experiments. (a) Hsc70: Solid curve shows results of double-exponential fit to the data, with initial and final values of the curve constrained to be equal to steady-state values of R_g in presence of ATP and ADP, respectively, and with first rate constant equal to that of ATP hydrolysis. (b) 60 kDa fragment: Solid curve shows result of double-exponential fit to the data. ATP hydrolysis under single-turnover conditions is shown in open circles with a single-exponential fit (dashed curve).

experimental error and gives an estimate of the size of that error.

Kinetics of the Change in R_g. To determine the time course of the change in R_g, data were collected for both Hsc70 (March 1995) and the 60 kDa fragment (June 1994) after manual mixing of nucleotide-free protein with substoichiometric amounts of MgATP (80−90%). Because radiation damage precluded data collection for longer than 10 min (for the 60 kDa fragment, June 1994) or 20 min (Hsc70, March 1995) from a single sample, longer time courses were assembled by transferring an aliquot from a master reaction to the sample cell every 12 min (60 kDa fragment) or 22 min (Hsc70). The temperatures of both cell and master reaction were maintained at 25 °C. R_g values were computed for each 1 or 2 min accumulation of data (Figure 3). For both proteins, the minimum value of R_g has been reached at

the earliest data collection time (~1.5 min). The minimum R_g is equal to the steady-state value measured in the presence of excess MgATP. The observed R_g returned to the larger value, equal to (or larger than) that observed with excess MgADP in steady-state measurements, over the course of minutes.

The values of R_g^2 as a function of time were analyzed as a linear combination of the steady-state values of R_g^2 in the presence of MgADP and the presence of MgATP.[2] For Hsc70, estimating the rate of return to the larger R_g^2 by fitting a single exponential to the data gave a rate constant of 0.0012 ± 0.0001 s^{-1} ($t_{1/2}$ = 9.6 min). Under the conditions of these experiments (T = 25 °C), the rate constant for ATP hydrolysis is 0.0030 s^{-1} ($t_{1/2}$ = 3.8 min); the relaxation to the large R_g^2 is significantly slower than ATP hydrolysis. Therefore, the return of R_g^2 to the larger value was simulated as a two-step process, with the first step having the rate constant (k_{hyd}) of hydrolysis:

$$R_g^2(\text{apparent}) = R_g^2(\text{steady-state ADP}) - \Delta(R_g^2)\frac{k_{hyd}e^{-k_\beta t} - k_\beta e^{-k_{hyd}t}}{k_{hyd} - k_\beta}$$

where R_g^2(steady-state ADP) and $\Delta(R_g^2)$ are determined by steady-state measurements under conditions identical (except for nucleotide concentration) with those of the kinetic experiment (Figure 3a). This yields a value of 0.0019 ± 0.0003 s^{-1} ($t_{1/2}$ = 6.1 min) for the second rate constant, k_β.

Product release from Hsc70 is ordered (Ha & McKay, 1994); P_i dissociates first with $k_{off}(P_i)$ = 0.0038 s^{-1} ($t_{1/2}$ = 3.0 min); ADP then dissociates more rapidly with k_{off}(ADP) = 0.029 s^{-1} ($t_{1/2}$ = 0.4 min). The value of k_β determined here is significantly slower than the rates of product release. The possibility that this difference may be due to prep-to-prep variability in the protein cannot be ruled out; nor can it be ruled out that the difference is significant. Therefore, the return to the large R_g form of Hsc70 after binding of MgATP may coincide with, or may be a relaxation process predicated on, product release; it does not coincide with, and is too slow to be correlated with, ATP hydrolysis.

This conclusion is corroborated by the kinetics of the change of R_g of the 60 kDa fragment. The return to a larger R_g^2 could be fit as an exponential decay with rate constant 0.0009 ± 0.0002 s^{-1} ($t_{1/2}$ = 13 min), to be compared with a rate of hydrolysis of 0.0017 s^{-1} (Figure 3b). If a two-step process is used to model the data, using the ATP hydrolysis rate constant for the first step, then the second step has a rate constant of 0.0070 ± 0.0020 s^{-1} ($t_{1/2}$ = 1.6 min). For the 60 kDa fragment, release of both P_i and ADP is rapid compared to hydrolysis, so that it is not possible to discriminate between hydrolysis and product release as concisely as with Hsc70. However, it is clear that when a single ATPase cycle is initiated synchronously, the time required for the return to the larger R_g is no faster than the time required for hydrolysis and product release in the 60 kDa fragment.

[2] During the kinetic experiment, the protein is considered to be a mixture of two forms (ADP-bound and ATP-bound). The resulting scattering curve is then a linear combination of scattering curves from the two different forms. In the Guinier region, the slope of the linear falloff of ln(I) versus S^2 will be a linear combination of the slopes of Guinier plots for the two different forms; the slopes are proportional to the R_g^2 values.

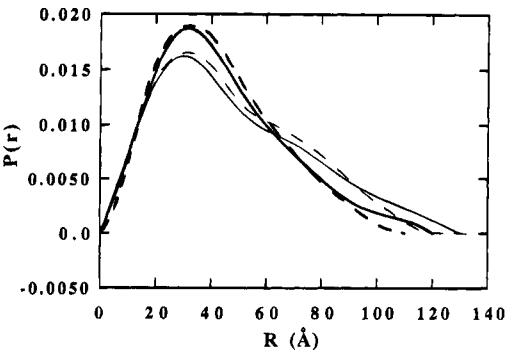

FIGURE 4: Distance distribution functions for Hsc70 in the presence of MgATP (boldface lines) and in the presence of MgADP (lightface lines), (−) experimentally derived from 4 mg/mL protein and (− − −) calculated from the monomeric box model.

At times >50 min in the kinetic experiments, Hsc70 reaches an R_g larger than that measured at steady state. It is not known whether this is due to aggregation of the sample, adoption of a third, even more extended conformation, or some other phenomenon.

Calculation of P(r) and R_g from Higher Angle Data. The values of R_g derived from the scattering data in the Guinier region suggest that Hsc70 is an elongated molecule; the measured values of R_g can be compared to a calculated value of ~21 Å that would be expected if Hsc70 were spherical. To acquire more information on the overall shape of Hsc70 and its subfragments, we collected data from each construct at 4 mg/mL with both the linear detector (which gives good resolution at low angle) and the quadrant detector (which gives greater signal at higher angle) and used the combined scattering curves to calculate $P(r)$ functions. In addition, $P(r)$ functions were calculated from data collected solely on the linear detector, including data outside the Guinier region, for samples at concentrations other than 4 mg/mL. Radii of gyration were calculated from the $P(r)$ functions. $P(r)$ functions computed using data from only the linear detector showed no significant differences from those computed using combined data to higher angle from the linear and quadrant detectors.

The $P(r)$ functions for Hsc70 (Figure 4) and the 60 kDa fragment (Figure 1b, insert) share several features which are consistent with elongated proteins that undergo substantial conformational changes. First, the d_{max} values (120−130 Å for Hsc70; 115−125 Å for the 60 kDa fragment) indicate that the molecules are elongated. Second, the $P(r)$ functions for both proteins in the presence of MgADP show distinct shoulders at 70−80 Å, suggestive of a bilobal shape. Third, the $P(r)$ functions for the proteins in the presence of MgATP reflect a substantial contraction relative to that for MgADP; the shoulders are much diminished, and the d_{max} values are substantially smaller (Table 1).

Modeling Based on P(r) Functions. $P(r)$ functions were used to construct a rudimentary model for Hsc70 and its subfragments. Initially, correspondence was established between the $P(r)$ function derived from scattering data and the $P(r)$ functions computed from crystallographic coordinates of the ATPase fragment. The crystallographic model of the ATPase fragment included amino acid residues 4−381, one ADP molecule, P_i, one Mg^{2+} ion, two K^+ ions, one Cl^- ion, and, in some calculations, the 205 H_2O molecules that

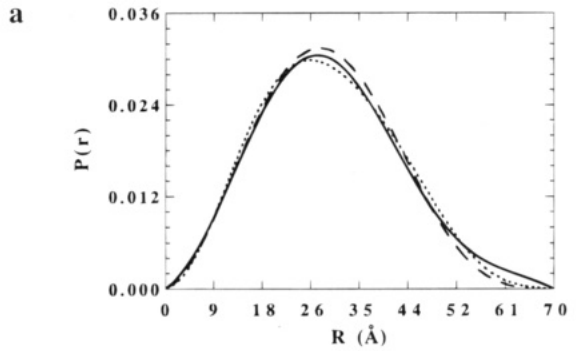

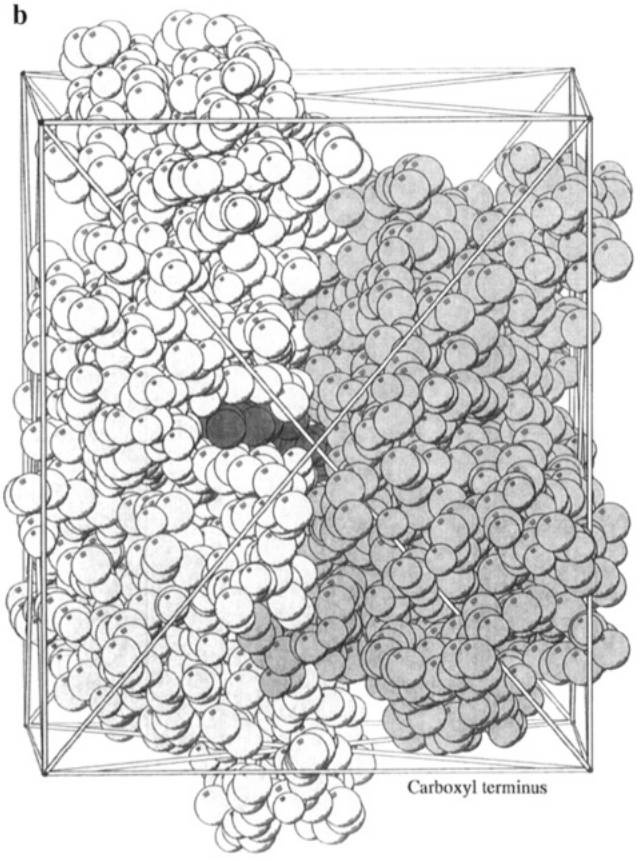

FIGURE 5: (a) Distance distribution functions for ATPase domain, (−) experimentally derived from 4 mg/mL protein in the presence of MgADP, (− − −) calculated from the box model, and (•••) computed from the crystal-derived coordinates of the ATPase domain, with hydration layer added. The experimentally derived $P(r)$ functions in the presence of MgATP are practically superimposable with the experimental curve shown. (b) Superposition of the 56 × 47 × 26 Å^3 box model of ATPase on a space-filling model of the ATPase domain, drawn with Molscript (Kraulis, 1991). Residues 4−182 and 363−381 are shown in light gray, residues 183−362 in white, and the bound nucleotide in dark gray.

are within 3.0 Å of protein, nucleotide, or cofactor atoms. The value of R_g calculated from these coordinates, with or without the 205 water molecules, was 21.0 Å; the $P(r)$ function computed from the coordinates showed significant disagreement with the function derived from experimental scattering data. However, addition of an appropriate layer of hydration (ca. 3 Å shell with an electron density value which is 0.03 e/Å^3 greater than that of solvent) to the crystallographic model, using the method of Svergun as implemented in the CRYSOL program package (Svergun *et al.*, 1995), yielded good agreement between both R_g (22.5 Å) and the overall $P(r)$ function (Figure 5a). We obtained a similar result—agreement between experimental and calculated $P(r)$ functions only when a layer of hydration is added to the crystallographic structure of the molecule—for a second test case, lysozyme, using data collected during these experiments (data not shown).

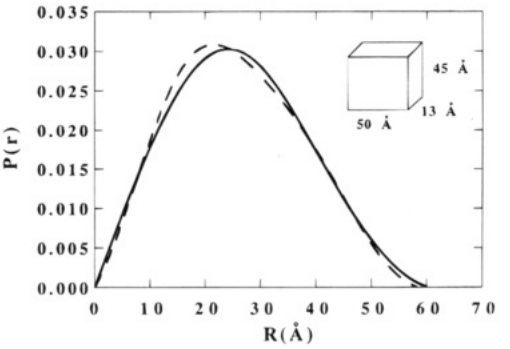

FIGURE 6: Distance distribution functions for the peptide-binding domain, (−) experimentally derived from 4 mg/mL protein and (− − −) calculated from the 50 × 45 × 13 Å^3 box model shown in the inset.

A rectangular solid (or box) was chosen as a simple (described by three parameters) and convenient geometric shape for modeling the ATPase domain. The R_g of a box with edge dimensions a, b, and c:

$$R_g^2 = (a^2 + b^2 + c^2)/12$$

was constrained to equal to the experimental value of R_g. The volume was set equal to the 1.4 × (protein molecular weight) × 1.21 Å^3/Da (average protein specific volume). The use of a volume 40% larger than that computed from the molecular weight results from the increase in volume upon addition of the 3 Å hydration shell necessary to bring the R_g and $P(r)$ functions calculated from "dry" atomic coordinates of the ATPase domain into agreement with SAXS data. Using these two constraints (R_g and volume), dimensions for a series of boxes were generated by allowing c to range 52−58 Å, varying the ratio of a:b from 1.0 to 2.5 in steps of 0.25, and choosing values of the three dimensions that gave the correct R_g and also had a d_{max} approximately equal to the experimental value. $P(r)$ curves were generated for the box models and normalized to the experimentally derived $P(r)$ (matching areas under each curve). The resulting $P(r)$ functions were compared visually to the experimentally derived function in order to select an optimal set of dimensions. Typically, variations of ~10% in box dimensions, subject to the constraints described above, showed little apparent difference in agreement between calculated and experimental $P(r)$ functions; larger variations showed clearly discernible differences.

The best dimensions found to model the ATPase domain in the presence of nucleotide were 56 × 47 × 26 Å^3. Superposition of such a box on the crystallographic structure encloses >90% of the protein atoms (Figure 5b). The $P(r)$ function computed for these dimensions shows reasonable agreement with the experimental curve and with that computed from hydrated atomic coordinates (Figure 5a).

The same method was used to determine dimensions of a box to represent the peptide-binding domain. The best values found for the peptide-binding domain were 50 × 45 × 13 Å^3 (Figure 6). These values support the qualitative judgment drawn from the shape of the $P(r)$ function that the peptide-binding domain is oblate rather than prolate.

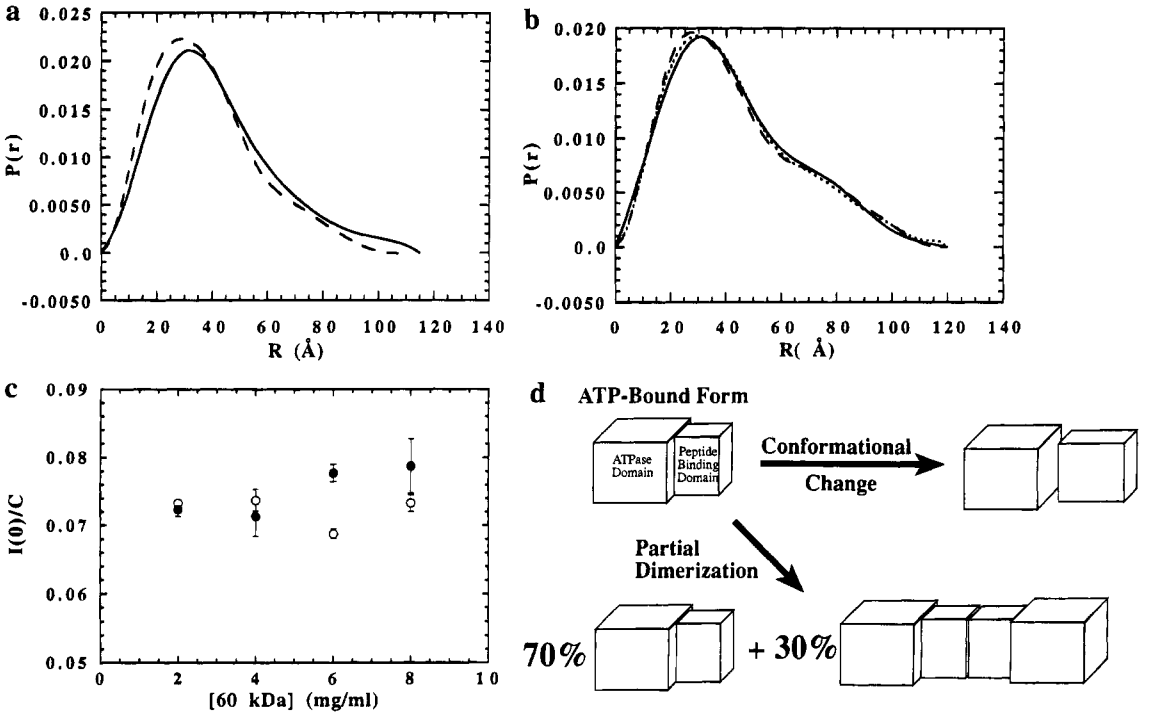

FIGURE 7: Distance distribution functions for the 60 kDa fragment (a) in the presence of MgATP and (b) in the presence of MgADP, (−) experimentally derived from 4 mg/mL protein, (− − −) calculated from the monomeric box model, and (• • •) calculated from the partial dimer box model. (c) $I(0)/c$ for the 60 kDa fragment in the presence of (●) MgATP and (○)MgADP. (d) Box models used for calculations in panels a and b. Two alternative ADP state models are shown; in the "partial dimerization" model, 30% of the protomers form dimers.

Two different schemes were used to model the 60 kDa fragment. First, it was modeled as a monomeric protein in both the ATP-bound and ADP-bound forms by combining the ATPase and peptide-binding domain models. This reduced the problem to determining (1) the separation between the two domains and (2) their relative orientations. The parallel axis theorem was used to derive an expression that determines the separation of the centers of mass of the ATPase and peptide-binding domains, given the R_g values of both domains and the 60 kDa fragment:

$$R_{g_{tot}}^2 = f_1 R_{g_1}^2 + f_2 R_{g_2}^2 + f_1 f_2 d^2$$

where f_1 and f_2 are the respective mass fractions and R_{g_1} and R_{g_2} the respective radii of gyration of the two domains, d is the separation between their centers of mass, and $R_{g_{tot}}$ is the R_g of the 60 kDa fragment. This analysis yields a separation of 58 Å for the ADP-bound form and 44 Å for the ATP-bound form of the 60 kDa fragment. To assess which relative orientations of the two domains are consistent with our data, a selection of orthogonal relative orientations was used with these separations to calculate $P(r)$ functions (shown in Figure 7). We did not require that the two domains be either in contact or not interpenetrating in this analysis. The $P(r)$ function for the ADP-bound form was particularly sensitive to alternative orientations of the two domains. Reasonable agreement was obtained with models having the short axes parallel to each other and perpendicular to the line through the centers of mass of the two domains (side-to-side, end-to-end, or end-to-side models). In contrast, any model having the shortest axis of one domain parallel to the line through the centers of mass of the two domains ("T-shaped", "L-shaped", and face-to-face models) did not agree well. The ATP-induced conformational change was then modeled as a contraction between the domains.

In the second scheme, we asked whether scattering data for the ADP-bound form of the 60 kDa fragment could be modeled as resulting from aggregation of a molecule that retained the overall structure and dimensions of the ATP-bound form. Hypothetical scattering curves for a mixed population of monomers and dimers were computed, with the dimers formed by placing the monomers face-to-face, side-by-side, or end-to-end. It was found that when *ca.* 30% of the protomers formed end-to-end dimers, the $P(r)$ function calculated from the hypothetical curve also showed good agreement with the experimentally derived $P(r)$ function (Figure 7b). The R_g value calculated from the resultant model $P(r)$ function was 34.7 Å, which agrees well with the experimental value of 34.3 Å. However, the R_g value calculated from the Guinier analysis of the model scattering curves was significantly higher, 37.8 Å, reflecting a lack of agreement at low angle between experimental scattering curves and those computed for a mixture of monomers and dimers.

In summary, agreement between experimental and model $P(r)$ functions for the ADP-bound form of the 60 kDa fragment can be achieved in two ways: either by inducing a large conformational change relative to the ATP-bound form and assuming the solution is completely monomeric or by introducing a significant fraction of dimerization in the solution. Arguments that may discriminate between these two alternatives are presented in the discussion.

To extend the modeling to Hsc70, alternative ways of adding ~10 kDa of protein to the peptide-binding fragment were tried. We got the best agreement of experimental and model $P(r)$ functions (Figure 4) when a box with dimensions 50 × 70 × 13 Å was used to represent the carboxy-terminal domain (residues 388−650); this is achieved by increasing the intermediate dimension of the box representing the

peptide-binding domain (dimensions 50 × 45 × 13 Å) by 25 Å.

Measurements on nucleotide-free ATPase fragment indicated a somewhat larger R_g (0.6 Å) in the absence of nucleotide than in the presence of either MgATP or MgADP, suggesting that a "hexokinase-like" opening of the nucleotide-binding cleft may occur upon release of nucleotide (Fletterick *et al.*, 1975; Bennett & Steitz, 1980). An increase in the R_g of the 60 kDa fragment in absence of nucleotide was not observed; this is not unexpected, since (if the center-to-center distance of the ATPase and peptide-binding domains remained essentially unchanged when nucleotide was released) only a 0.3 Å increase in R_g would be expected for this fragment for a conformational change that increased R_g of the ATPase fragment by 0.6 Å.

DISCUSSION

The results presented support the conclusions: (1) the ATPase and peptide-binding fragments are relatively oblate; they are linked in a manner that forms a markedly elongated and prolate 60 kDa fragment and full-length Hsc70; (2) MgATP induces a substantial decrease in R_g in both Hsc70 and the 60 kDa fragment, relative to their MgADP-bound forms; and (3) the transition to the ATP-induced conformation occurs more rapidly than ATP hydrolysis and presumably results from some step of ATP binding, while the rate of the reverse transition to the more elongated state correlates with product release.

Scattering curves measured under steady-state conditions for the 60 kDa fragment and its constituent domains provide the information necessary to construct "low-resolution" models for these fragments. Reliability of the modeling methodology is evidenced by the agreement of the "box" model for the ATPase fragment with the overall dimensions of the crystallographic structure and the agreement of both the box model and the crystallographic structure with the experimental scattering curves, as long as a ~3 Å layer of hydration is added to the crystallographic coordinates. These schematic models, taken in conjunction with the crystallographic structure of the ATPase fragment, show that a relatively flat peptide-binding fragment probably interacts either end-to-end or side-to-side with the ATPase fragment in the ATP-induced form of the molecule. They exclude models in which the peptide-binding domain folds directly onto, and interacts extensively with, the largest faces of the ATPase domain.

Figure 7d shows schemes of the two alternative hypotheses used to model the large increase in R_g that occurs going from the ATP-bound forms to the ADP-bound forms of the 60 kDa fragment and Hsc70: (1) a large conformational change within monomeric molecules versus (2) partial dimerization (*e.g.*, ~30% of the protomers) of the molecules. It should be emphasized in this regard that the scattering curves do not display an upswing at low angle that would be indicative of nonspecific, heterogeneous aggregation (Figure 1).

The partial dimerization model is appealing as Hsc70 can be isolated in a dimeric form which can be dissociated with ATP (Schlossman *et al.*, 1984; Freiden *et al.*, 1992). However, there are several arguments against the dimerization model for the large ΔR_g we observe. First, partial dimerization would increase the average molecular weight for the ensemble of molecules, and this increase would be detectable as an increase in $I(0)/c$ (intensity at zero scattering angle over concentration). For example, if 30% of the molecules dimerize, an increase of ~30% in $I(0)/c$ is expected.[3] However, although the sample-to-sample variation of the experimental values for this parameter is relatively large (~5−10%) over extended periods of data collection, due to variations in beam intensity and detector response, we do not observe systematically larger values in the presence of ADP versus ATP on samples that are otherwise identical and on which measurements are made close in time (Figure 7c).

Second, if the larger R_g in the presence of ADP is the result of dimerization, this should be reflected in the dependence of R_g on protein concentration; R_g should increase significantly with increasing protein concentration and extrapolate to approximately the same value at zero concentration as seen with ATP-bound protein. However, the steady-state R_g versus concentration has a similar, approximately level trend in the presence of both ADP and ATP for both Hsc70 and the 60 kDa fragment (Figure 2). Also, calculations show that the R_g computed in the Guinier approximation would be larger than that computed from the $P(r)$ function; this is not the case (Table 1).

Third, two different biochemical tests support our ability to isolate stable monomers of the 60 kDa fragment. Native gels of samples of the 60 kDa fragment in its ADP-bound form show only minor amounts (<1%) of dimer. Hsc70 is more problematic; gels of Hsc70 show significant aggregation after storage for extended periods of time. Dynamic light scattering from samples of monomeric Hsc70 did not show polydispersity and showed a substantially smaller hydrodynamic radius compared to a sample purified as dimer.

Fourth, when scattering curves were collected repetitively on samples of the 60 kDa fragment over many hours, the computed values of R_g remained stable. In contrast, experiments with Hsc70 showed an increase in R_g by 20 h, consistent with results of gel filtration showing that significant aggregation occurs with full-length protein after storage in solution for this amount of time.

Hence, although we can model the $P(r)$ function of the ADP-bound 60 kDa fragment with a sample that is a mixture of monomers and dimers of the protein in its ATP-bound conformation, we do not see the effects we would expect from dimerization on values of $I(0)/c$ or on the concentration and time dependence of R_g. Nor do we see biochemical evidence for substantial aggregation of the 60 kDa fragment. It is notable in this regard that taken by itself, the evidence on Hsc70 is less compelling. While $I(0)/c$ shows no dimerization of Hsc70 in the presence of ADP, we see substantial variation in measured values of R_g as well as biochemical evidence for significant aggregation over time. We have tried to minimize the effect of this on our experiments by minimizing the amount of time between gel filtration of Hsc70 samples and scattering measurements on them. The arguments discussed above, which rely more heavily on data from the 60 kDa fragment than on data from Hsc70, favor a large, ATP-induced conformational change over partial dimerization as an explanation for the large ΔR_g that is observed in both proteins.

[3] Since $I(0) \propto (MW)^2$ for each molecule, if α is the fraction of protomers that form dimers, then for a mixture $I(0) \propto (1 - \alpha)(MW)^2 + (\alpha/2)(2MW)^2 = (1 + \alpha)(MW)^2$ since $N\alpha$ protomers form $N\alpha/2$ dimers, where N is the total number of molecules.

Regardless of which particular model ultimately proves correct, we discern two significantly different conformational states for both Hsc70 and the 60 kDa fragment by solution scattering. The state with the larger R_g is observed under several sets of conditions, including (i) absence of nucleotide, (ii) presence of saturating levels of MgADP, (iii) presence of slowly hydrolyzable ATP analogs, AMPPNP or AMPPCP, and (iv) with MgATP in the presence of 100 mM Na^+ rather than K^+ as a monovalent counterion. The ATP-induced state is observed only in the presence of MgATP with K^+. This correlates with observations from other laboratories that MgATP induces a conformational change in stress-70 proteins but slowly hydrolyzable ATP analogs fail to do so, and presence of K^+ is also required to achieve this conformational change (Liberek *et al.*, 1991; Banecki *et al.*, 1992; Palleros *et al.*, 1992, 1993).

Although these data demonstrate two different conformational states for Hsc70 and the 60 kDa fragment, it should be noted that the values of steady-state R_g measured in the presence of saturating levels of MgATP represent a mixture of states. Under these conditions, all enzymatic intermediates of the ATPase cycle will be present, and the fraction of each intermediate in solution will be equal to the fraction of time that each molecule spends in that state during the enzymatic cycle. For the 60 kDa fragment, the kinetic constants for the ATPase cycle demonstrate that the majority of the molecules will have MgATP bound under the steady-state conditions used in the scattering experiments. ATP binding is rapid ($\tau_{1/2} < 1$ s), hydrolysis is the rate-limiting step of the cycle ($\tau_{1/2} = 400$ s), and following hydrolysis, products are released rapidly ($\tau_{1/2} < 100$ s), allowing ATP to rebind. Thus ≥80% of the 60 kDa fragment molecules will have ATP bound. By implication, since the structural transition to the ATP-induced conformation is apparently brought about by ATP binding, while the reverse transition is predicated on ATP hydrolysis or product release, ≥80% of the molecules will be in the more compact, ATP-induced conformation in steady-state experiments. This correlates with the observation that, when the transition is synchronized by mixing stoichiometric amounts of MgATP and the 60 kDa protein, the R_g at $t = 0$ (27.7 ± 0.5 Å, estimated from a double-exponential fit to R_g versus time), when essentially all of the protein should be in the ATP-induced conformation, equals that observed with MgATP in steady-state experiments (27.9 ± 0.5 Å).

For Hsc70, the ATP hydrolysis and P_i release steps require approximately equal time ($\tau_{1/2} = 240$ and 180 s, respectively), while ADP release is relatively rapid ($\tau_{1/2} = 24$ s). In the presence of excess MgATP, Hsc70 will be an *ca.* 50:50 mixture of protein with ATP bound and protein with ADP + P_i bound. Depending on whether ATP hydrolysis or, alternatively, P_i or ADP release facilitates the transition from the compact to the more elongated state, Hsc70 would be either a ~50:50 mixture of protein in two different conformations or, alternatively, >90% in the ATP-induced form. The kinetics of the change of R_g after mixing stoichiometric amounts of Hsc70 and MgATP show that the R_g observed at early times is equal within error to that observed with MgATP under steady-state conditions, demonstrating that the transition to the elongated form is predicated on product release rather than on ATP hydrolysis. The rate constant inferred from our data is consistent with this interpretation.

The conformational switch which induces the transitions between the two states presumably relies on the ability of nucleotide, which binds at the base of a cleft in the ATPase domain, to transmit a conformational shift to the periphery of this domain. However, no major change in R_g is observed between the ATP-bound and ADP-bound 44 kDa ATPase fragment. This argues that any ATP-induced conformational change in this fragment is relatively subtle. An increase in R_g is observed in the absence of nucleotides, suggesting that the cleft of the ATPase fragment opens when nucleotide is released. However, this does not appear to correlate with the transition to or from the ATP-induced state.

When modeled as a large conformational change in a monomeric 60 kDa fragment, the change from the ATP-induced state to the more elongated ADP-bound state involves an increase of the center-to-center distance between the two domains of ~14 Å. This suggests that the ATPase and peptide-binding domains disassociate and may have a few if any noncovalent interactions in the more extended state. These conclusions can be extended to Hsc70, whose behavior is similar to that of the 60 kDa fragment. The solution scattering data demonstrate that, at the level of substantial structural changes in the protein, the 60 kDa fragment mimics Hsc70. A caveat to be emphasized at this point is that the carboxy-terminal ~100 amino acid residues of Hsc70 that are not present in the 60 kDa fragment may be involved in significant interactions to which the solution scattering experiments, being relatively coarse in resolution, are not sensitive.

The low-peptide-affinity state of DnaK characterized by Palleros *et al.* shares two significant features with the ATP-induced state described here: (1) both are induced by ATP before hydrolysis occurs and (2) both appear to persist for a matter of minutes (Palleros *et al.*, 1993). Although it is appealing and reasonable to suggest that the two different states observed in Hsc70 and the 60 kDa fragment correspond to the high-peptide-affinity and low-peptide-affinity states of the proteins, this has not been demonstrated directly. Experiments are currently underway to determine whether this suggestion is correct.

A question which remains to be addressed is, which chemical steps of the ATPase cycle transduce the conformational changes? The transition to the ATP-induced structure both in the 60 kDa fragment and in Hsc70 occurs more rapidly than ATP hydrolysis and appears to be correlated with ATP binding. Crystallographic work on the wild-type ATPase fragment shows how both AMPPNP and ADP + P_i bind to this fragment. These structures, along with structures of several mutants with either ATP or ADP + P_i bound, show both a "prehydrolysis" state and "posthydrolysis" state for the nucleotide. There is no significant difference in the overall tertiary structure of the ATPase fragment between these two states. To the extent the crystallographic structure of the isolated ATPase fragment represents its structure in conjunction with the peptide-binding domain in Hsc70 and the 60 kDa fragment, this suggests that it must have an additional (that is, not yet crystallized) conformational state that is accessed by ATP but not by AMPPNP. It appears that AMPPNP is unable to stabilize the ATP-induced state in either crystal or solution studies. In the hydrolysis pathway proposed for ATP, the nucleotide first binds in the same manner as AMPPNP and then rearranges to allow the phosphates to form a β,γ-

bidentate complex with the Mg^{2+} ion in the active site. Hydrolysis then proceeds by an in-line attack mechanism. By inference, the postulated β,γ-bidentate complex of ATP is a candidate for a specific ATP conformation which provokes a structural shift which is then transduced from the nucleotide to the periphery of the ATPase fragment.

As for the step which precedes the converse structural transition, from the ATP-induced state to the more elongated state, our current data limit the possibilities to product release but cannot discriminate between P_i or ADP release for this role; both are equally viable candidates for the biochemical step that triggers a conformational change. In the context of the structural similarity of the Hsc70 ATPase fragment with actin, it is intriguing to raise the question of whether P_i release induces a subtle shift in the ATPase domain of Hsc70 that destabilizes the interactions with the peptide-binding domain, in the same manner that P_i release apparently induces a subtle structural change in actin that destabilizes the protein−protein interactions in the actin filament (Korn *et al.*, 1987).

ACKNOWLEDGMENT

We wish to gratefully acknowledge the assistance of Lauren Shirvanee, Libby Morimoto, and Samina Taha with sample preparation, Drs. Eric Johnson and Shigeki Takeda with data collection and discussions, and advice from Drs. David Eliezer and Jeung-Hoi Ha.

REFERENCES

Banecki, B., Zylicz, M., Bertoli, E., & Tanfani, F. (1992) *J. Biol. Chem. 267*, 25051−25058.

Beckmann, R. P., Mizzen, L. A., & Welch, W. J. (1990) *Science 248*, 850−854.

Bennett, W. S. J., & Steitz, T. A. (1980) *J. Mol. Biol. 140*, 211−230.

Blond-Elguindi, S., Cwirla, S. E., Dower, W. J., Lipshutz, R. J., Sprang, S. R., Sambrook, J. F., & Gething, M. J. (1993) *Cell 75*, 717−728.

Chappell, T. G., Welch, W. J., Schlossman, D. M., Palter, K. B., Schlesinger, M. J., & Rothman, J. E. (1986) *Cell 45*, 3−13.

Chappell, T. G., Konforti, B. B., Schmid, S. L., & Rothman, J. E. (1987) *J. Biol. Chem. 262*, 746−751.

Chirico, W. J., Waters, M. G., & Blobel, G. (1988) *Nature 332*, 805−810.

Deshaies, T. J., Koch, B. D., Werner-Washburne, M., Craig, E. A., & Schekman, R. (1988) *Nature 332*, 800−805.

Flaherty, K. M., DeLuca-Flaherty, C., & McKay, D. B. (1990) *Nature 346*, 623−628.

Flaherty, K. M., McKay, D. B., Kabsch, W., & Holmes, K. C. (1991) *Proc. Natl. Acad. Sci. U.S.A. 88*, 5041−5045.

Fletterick, R. J., Bates, D. J., & Steitz, T. A. (1975) *Proc. Natl. Acad. Sci. U.S.A. 72*, 38−42.

Flynn, G. C., Chappell, T. G., & Rothman, J. E. (1989) *Science 245*, 385−390.

Flynn, G. C., Pohl, J., Flocco, M. T., & Rothman, J. E. (1991) *Nature 353*, 726−730.

Freiden, P. J., Gaut, J. R., & Hendershot, L. M. (1992) *EMBO J. 11*, 63−70.

Gething, M. J., & Sambrook, J. (1992) *Nature 355*, 33−45.

Gragerov, A., Zeng, L., Zhao, X., Burkholder, W., & Gottesman, M. E. (1994) *J. Mol. Biol. 235*, 848−854.

Guinier, A. (1963) *X-ray Diffraction in Crystals, Imperfect Crystals, and Amorphous Bodies*, W. H. Freeman & Co., San Francisco, CA.

Ha, J.-H., & McKay, D. B. (1994) *Biochemistry 33*, 14625−14635.

Kim, D., Lee, Y. J., & Corry, P. M. (1992) *J. Cell. Physiol. 153*, 353−361.

Korn, E. D., Carlier, M.-F., & Pantaloni, D. (1987) *Science 238*, 638−644.

Kraulis, P. (1991) *J. Appl. Crystallogr. 24*, 946−950.

Langer, T., Lu, C., Echols, H., Flanagan, J., Hayer, M. K., & Hartl, F.-U. (1992) *Nature 356*, 683−689.

Liberek, K., Skowyra, D., Zylicz, M., Johnson, C., & Georgopoulos, C. (1991) *J. Biol. Chem. 266*, 14491−14496.

Morshauser, R. C., Wang, H., Flynn, G. C., & Zuiderweg, E. R. P. (1995) *Biochemistry 34*, 6261−6266.

O'Brien, M. C., & McKay, D. B. (1993) *J. Biol. Chem. 268*, 24323−24329.

Palleros, D. R., Reid, K. L., McCarty, J. S., Walker, G. C., & Fink, A. L. (1992) *J. Biol. Chem. 267*, 5279−5285.

Palleros, D. R., Reid, K. L., Shi, L., Welch, W. J., & Fink, A. L. (1993) *Nature 365*, 664−666.

Pelham, H. R. B. (1986) *Cell 46*, 959−961.

Rice, M., & Wakatsuki, S. (1991) *SSRL/SLAC user manual*, Stanford Synchrotron Radiation Laboratory, Stanford, CA.

Scherer, P. E., Krieg, U. C., Hwang, S. T., Vestweber, D., & Schatz, G. (1990) *EMBO J. 9*, 4315−4322.

Schlossman, D. M., Schmid, S. L., Braell, W. A., & Rothman, J. E. (1984) *J. Cell. Biol. 99*, 723−733.

Semenyuk, A. V., & Svergun, D. I. (1991) *J. Appl. Crystallogr. 24*, 537−540.

Svergun, D. I., Barberato, C., & Koch, M. H. J. (1995) *J. Appl. Crystallogr.* (submitted for publication).

Wakatsuki, S., Hodgson, K. O., Eliezer, D., Rice, M., Hubbard, S., Gillis, N., & Doniach, S. (1992) *Rev. Sci. Instrum. 63*, 1736−1740.

Wang, T., Chang, J., & Wang, C. (1993) *J. Biol. Chem. 268*, 26049−26051.

Wilbanks, S. M., DeLuca-Flaherty, C., & McKay, D. B. (1994) *J. Biol. Chem. 269*, 12893−12898.

BI9513970